Fully automated estimation of fMRI guided SPECT brain networks and their functional network connectivity in schizophrenia patients vs controls: a NeuroMark ICA approach

Amritha Harikumar[1], Maria Misiura[1], Daniel Amen[3,4], David Keator[2,3,4], Vince D. Calhoun[1]

[1] Tri-Institutional Center for Translational Research in Neuroimaging and Data Science (TReNDS), Georgia State, Georgia Tech, Emory, Atlanta, GA
[2] Psychiatry and Human Behavior, University of California, Irvine, Irvine, CA.
[3] Change Your Brain Change Your Life Foundation, Costa Mesa, CA.
[4] Amen Clinics Inc., Costa Mesa, CA.

Key words: Functional network connectivity, schizophrenia, psychosis, networks, SPECT

Abstract

Single photon emission computerized tomography (SPECT) scans have emerged as a useful imaging modality that has been explored in the literature for the last 40 years. To date, little work has focused on studying functional network connectivity utilizing SPECT data. In this study, we present a fully automated, spatially constrained ICA (sc-ICA) approach to evaluate functional network connectivity profiles in SPECT data using the NeuroMark pipeline. We then use this to compare group differences in brain function in patients with schizophrenia (SZ) and healthy controls (HC). We evaluate both the expression of brain networks as well as the whole brain SPECT connectome (assessed as inter-subject covariation among networks) to evaluate the neuroimaging links to schizophrenia. 76 healthy controls, and 137 schizophrenia patient SPECT images were acquired from Amen Clinic sites along with diagnostic information. Each patient participated in two SPECT brain scans, acquired during rest and while performing a sustained attention task across twelve clinical imaging sites. Preprocessed SPECT data were analyzed via sc-ICA using 53 spatial priors derived from functional MRI data. Results revealed group differences between healthy controls and patient SPECT data. Out of the 53 components in the resting state SPECT data, 15 total components were found to show differences in various brain regions after correcting for multiple comparisons. The vast majority of components showed reduced connectivity in patients. Relationships were associated with age, sex, hearing voices and having disjointed thoughts. Additional covariates such as medication status and scanner type were considered. Initial associations with clinical variables revealed relationships between the auditory, sensorimotor, and cognitive control networks, as well as broad network connectivity between the cortical and default mode network areas. For the task data, the components found in resting data were replicated, with patients showing reduced connectivity in similar regions irrespective of task performance. In summary, these results confirm and extend existing work highlighting large scale network disruptions noted in prior schizophrenia fMRI studies between the subthalamic, cortical and auditory networks.

Introduction

Overview

Various neuroimaging methodologies such as single photon emission computerized tomography (SPECT) and functional magnetic resonance imaging (fMRI) scans have been used to capture clinically meaningful differences in psychiatric populations. Measuring blood oxygenation level dependent (BOLD) fMRI signals have resulted in many important findings, such as classifying depressive symptoms [1], as well as understanding more specific aspects, such as the functional architecture in the brain [2]. Correlating BOLD activation at rest across brain regions (i.e. resting state fMRI functional connectivity [3]) has identified a number of canonical functional connectivity patterns/networks that replicate and correspond to various functional domains [4,5,6].

Technitium-99 is a nuclear medicine-based neuroimaging approach which provides signal primarily related to blood flow. Blood flow is related to the BOLD fMRI signal, and has been utilized in SPECT studies [7] while providing insights into brain perfusion [8]. Importantly, cerebral blood flow (CBF) is a measurement of physiological activity; consequently, the relationship between blood flow and behavior have been considered in relation to psychiatric symptoms in disorders. More specifically in SPECT literature, perfusion (another name for blood flow [9]) has been linked with positive and negative symptoms in schizophrenia[10, 11, 12].

Studies have shown relationships between CBF and antipsychotic medication in first episode psychotic patients (FEP[12]), as well as key differences between reward processing, default mode, and language processing in patient groups such as schizophrenia vs. depressed subjects [13]. Given these findings, perfusion can be considered a robust measure in identifying brain-behavior relationships.

To this end, SPECT has been used to broadly study neuropsychiatric disorders [14] and also to identify regions linked to disorders such as neurodegenerative parkinsonisms [15]. While resting fMRI studies have extensively focused on brain networks, SPECT studies have typically utilized voxel wise correlations for clinical research, for example in cardiac studies [16] as well as Parkinson's disease utilizing machine learning [17, 18]. These studies investigating macro-scale brain networks across disorders can provide insights into covariation among brain regions and allow identification of network specific disruptions linked to brain disorders.

Multivariate techniques such as independent component analysis (ICA) which identify covarying components/networks in the brain have been widely utilized to identify possible biomarkers pertaining to various psychiatric disorders, including schizophrenia [19,20,21]. ICA is a technique which allows the extraction of components from functional brain networks to understand which parts of the brain are most active both at rest and while performing a task. [22] ICA, a type of blind

source separation, was originally used to solve the "cocktail party phenomenon" where signals from a source (e.g. speech signals) could be separated and unmixed to understand each individual source of noise [23, 69] .

Since it's inception, ICA has been adapted to understand individual sources of signal in brain imaging data [24,25]. Using ICA allows for more precise estimation of functional brain networks, as well as differentiation of brain networks related to function (e.g. differentiating bipolar, schizophrenia, and healthy controls from each other based on task based fMRI data)[26]. ICA has also been used to extract covarying networks in various modalities including structural MRI [27], subject level fMRI activation, or amplitude of low frequency fluctuation maps [22], positron emission tomography (PET) data[28,29], and in one case, SPECT data [15]. ICA has also been widely used to identify brain regions that exhibit coherent fluctuations, i.e., functional connectivity, captured in the spatial maps of each component in resting state fMRI data. Using ICA to study dysfunction in schizophrenia has yielded useful results, including identifying functional dysconnectivity between subgroups [30]. ICA has proven a powerful tool for identifying differences in connectivity patterns with high specificity that would otherwise be undetected using other methods [31].

More recently, the use of spatially constrained ICA (scICA) using a template based approach to further understand FNC across various disorders allows for a

fully automated ICA approach, allowing for comparability across studies while also capturing individual subject heterogeneity [32]. Spatially constrained ICA has yielded meaningful and exciting results, specifically understanding improved feature classification across disorders. The scICA NeuroMark pipeline has successfully identified unique brain impairments in schizophrenia and autism, with high classification accuracy that distinguishes clinical disorders such as bipolar disorder and major depressive disorder, and has also shown changes in the brain in individuals with Alzheimer's disease [33]. Capturing unique, more accurate features across diagnostic profiles could assist in more precise clinical diagnoses for clinicians, such as distinguishing schizophrenia from schizophreniform or bipolar disorders.

fMRI studies have notably focused on intrinsic brain networks, which have been particularly helpful in identifying wide spread patterns of dysconnectivity especially in disorders such as schizophrenia [20]. Schizophrenia is a multifaceted, complex disease with no known specific cause as to its onset. To understand specific network related dysfunctions in this disease, various studies have investigated the FNC between different networks that are disrupted in schizophrenia. Few studies to date have focused on evaluating brain networks estimated from SPECT imaging and understanding their relationship to clinical and cognitive variables related to schizophrenia. A notable gap in the literature is the

lack of approaches to provide useful and detailed information about how mental illness impacts covarying brain networks in SPECT data.

Additional gaps in the literature include comparing SPECT with fMRI findings, particularly with regard to clinical symptoms such as auditory hallucinations. A key feature in schizophrenia, studies have shown robust findings linking auditory hallucinations to particular brain regions related to visual, memory, and language areas. These areas include Broca's area, superior temporal gyrus (STG), putamen, and hippocampus, all which demonstrate dysconnectivity broadly which relate to hallucination symptoms in patients [34–38]. Broader PET and SPECT studies have noted other widespread brain regions associated with hallucinations, including the inferior frontal gyrus, cerebellum, parahippocampus and thalamus showing increased perfusion activity when patients experienced hallucinations [39]. Although hallucinations have been extensively studied using various imaging approaches, few studies exist which explicitly compare fMRI and SPECT based approaches to identify if similar perfusion activity is noted while patients experience hallucinations. More specifically, little research has identified whether a comparative approach between fMRI and SPECT yield identification of similar ICNs and ICs in auditory hallucination based brain regions and networks.

The purpose of this current study was to study group differences in patients with schizophrenia and healthy controls using fully automated, whole brain fMRI

guided scICA applied for the first time on SPECT data. We evaluated both the individual subject expression of spatial brain networks as well as the whole brain SPECT connectome (assessed as covariation among subjects) to understand neuroimaging links to schizophrenia. Additionally, we looked at the relationships between loading parameters in patients compared to clinical symptoms, and demographic covariates such as age and sex. By utilizing insights from previous fMRI studies as well as the NeuroMark template, our goal was to analyze SPECT data to study differences in network covariation within a large clinical sample of schizophrenia patients versus controls. We expect that based on previous fMRI studies utilizing NeuroMark, aberrant / disrupted connectivity will be identified in auditory, subcortical and thalamocortical networks [40,41]. We also expect to see disrupted connectivity in other large scale brain networks, such as the default mode network [42] , with specific relationships, such as associations noted between positive symptoms (i.e. hallucinations) and dysconnectivity broadly across these large scale networks.

Methods

SPECT Imaging Procedure and Preprocessing

76 healthy controls, and 137 schizophrenia patient SPECT images were acquired from Amen Clinics (https://www.amenclinics.com/). We provide a demographic of subjects in both healthy controls and patients (Table 1a). Race classification was done based on the Center for Disease Control's guidelines for race reporting (https://www.cdc.gov/nchs/hus/sources-definitions/race.html).

Amen Clinic Site #	Age (Mean | SD)	Subject Breakdown	Gender	Categorization
1	25 | 8.48 | 2 subject	2M	N/A	1 Hispanic/Latino , 1 African/American
2	31.77 | 11.08 | 35 subjects	17F/18M	48%/51%	1 Arab, 3 Asian, 19 Caucasian, 5 Hispanic/Latino, 1 Multiethnic, 1 Other, 5 Unknown
3	38.5 | 12.58 | 12 subjects	2F/10M	16.6%/83.3%	11 Caucasian, 1 Unknown
4	33.14 | 13.67 | 27 subjects	3F/24M	11.1%/88.88%	2 African/American, 23 Caucasian, 1 Hispanic/Latino, 1 Unknown
5	37.66 | 16.46 | 12 subjects	6F/6M	50%/50%	2 Asian, 8 Caucasian, 1 Native American, 1 Other
6	25.77 | 2.90 | 9 subjects	6F/3M	66.6%/33.3%	6 Caucasian, 1 Hispanic/Latino, 1 Other, 1 Unknown
7	34.10 | 15.32 | 19 subjects	4F/15M	21.05%/78.94%	1 African, 1 Asian, 15 Caucasian, 2 Unknown
8	32.54 | 11.08 | 11 subjects	6F/5M	54.54%/45.45%	2 Asian, 6 Caucasian, 1 Hispanic/Latino, 1 Other, 1 Unknown
10	30.16 | 10.22 | 6 subjects	2F/4M	33.33%/66.66%	4 Caucasian, 1 Multiethnic, 1 Unknown
11	69 | N/A (just 1 subject)	1F	N/A	1 Caucasian
12	33 | N/A (just 1 subject)	1F	N/A	1 Caucasian
13	43 | 22.62 | 2 subjects	1F/1M	50%/50%	2 Caucasian
	Total: 137 patients			

Amen Clinic Site #	Age (Mean | SD)	Subject Breakdown	Gender	Categorization
2	36 | N/A | 1 subject	1M	N/A	African American
2	48.71 | 6.92 | 7 subjects	4M/3F	57.14%/42.85%	Arab/Middle Eastern
2	29.28 | 6.92 | 7 subjects	3M/4F	42.85%/57.14%	Asian
2	43.74 | 17.94 | 55 subjects	32F/23M	58.18%/41.81%	Caucasian
2	35.33 | 9.266 | 6 subjects	3F/3M	50%/50%	Hispanic/Latino
	Total: 76 controls			

Table 1a. Demographic information for patients with schizophrenia and healthy controls from the Amen Clinic dataset, with the site breakdown, average age and standard deviation, along with race classification information across sites. 12 sites were included in this study. Healthy controls were all from Site 2.

Healthy participants were recruited under a prior study of SPECT in healthy participants and approved by Western IRB (WIRB # 20021714), with all participants consented (Integ Review Board #004-Amen Clinics Inc). Participants were excluded from the original study if they, or their first-degree relatives, had suicidal behavior, unstable medical conditions, epilepsy, any history of mental illness, head injury or other neurological disorders, dementia, mental retardation, or substance abuse/dependence disorders. All twelve sites had varying camera types depending on the scanner type (detailed below), with the same data acquisition parameters in line with Amen Clinic regulatory procedures. Adult participants were scanned with the following dosage amounts calibrated by weight (Table 1b):

Weight Range	Dosage Information of TC-99
<150-175 lbs	20 mCi
175-200 lbs	22.5 mCi
>200 lbs	25.0 mCi

Table 1b. Dosage information and calibration according to adult participant's weight; dosage amounts are in millicuries (mCi).

Each patient participated in two SPECT brain scans, acquired during rest and while performing a Conners Continuous Performance Test (Conners Continuous Performance Test, CCPT-II, Multi-Health Systems, Toronto, Ontario [43]) across twelve clinical imaging sites. Scans were performed between 2004 – 2022. SPECT scans were acquired using a Picker (Philips) Prism XP 3000 double-headed gamma camera (Picker Int. Inc., Ohio Nuclear Medicine Division, Bedford Hills, OH, USA) as well as the PRISM3000 triple-headed gamma camera (Picker Int. Inc., Ohio Nuclear Medicine Division, Bedford Hills, OH, USA) with low energy high resolution fan beam collimators. Participants were scanned across both types of scanners across the twelve sites. Scanning was completed prior to any diagnoses or treatment. For each procedure, an age- and weight-appropriate dose of 99mTc–hexamethylpropyleneamine oxime (HMPAO) was administered intravenously at rest. For the rest scans, patients were injected while they sat in a dimly lit room with their eyes open. Patients were scanned for approximately 30 minutes after injection. Data acquisition yielded 120 images per scan with each image separated by three degrees, spanning 360 degrees. A low pass filter was applied with a high cutoff and

Chang attenuation correction performed [44,45]. The resulting reconstructed image matrices were 128x128x78 with voxel sizes of 2.5mm^3.

For voxel-based analyses, images were aligned to the Montreal Neurological Institute (MNI) space with the advanced normalization tools (ANTs version 2.2.0[46], RRID:SCR_004757) using a SPECT template, resulting in an image matrix size of 79×96×68 with isotropic voxel sizes of 2.0mm^3. SPECT images were scaled to the within-scan maximum voxel and noise outside of the brain was removed using a 50% of maximum threshold, prior to registration. After the thresholded images were aligned to the MNI space and the transformation applied to the un-thresholded images, a brain mask derived from the MNI 152 [47,48] template was used to remove noise outside the brain from the un-thresholded images for use in the statistical models. Registered SPECT scans were visually checked for the absence of severe functional abnormalities or artifacts and proper registration to the MNI space.

ICA Processing

Preprocessed SPECT data were analyzed via spatially constrained ICA using the NeuroMark ICA template through the Group ICA of fMRI Toolbox (GIFT; http://trendscenter.org/software/gift; RRID:SCR_001953) run with MATLAB R2020b[49] (Version 9.9.0.2037887). SPECT scans from 213 subjects total (healthy controls and patients combined) were analyzed via the MOO-ICAR algorithm using

the NeuroMark fMRI 1.0 template (Table 2) which consisted of 53 ICs that replicated across two large scale human fMRI datasets (see Du et al., 2020 for a full breakdown of how the template was created, as well as more explanation regarding the MOO-ICAR approach)[50]. This resulted in 53 SPECT ICs as well as subject specific loading parameters. The 53 SPECT ICs included 7 independent component network (ICN) domains including the subcortical (SC), auditory (AUD), visual (VIS), sensorimotor (SM), cognitive control (CC), default mode network (DM), and cerebellar (CB) component regions for healthy controls and patients (Figure 1).

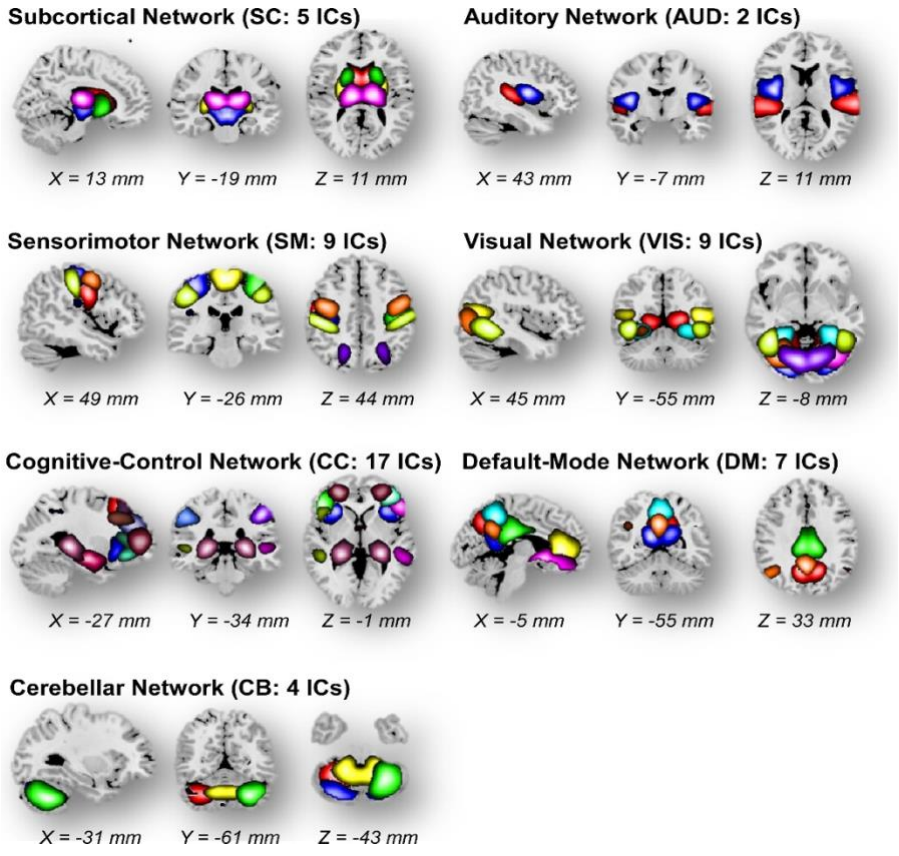

Figure 1. Adapted from Du et al., 2020 noting the 7 main ICNs used for the NeuroMark spatially constrained ICA analysis.

Independent Components as Regions of Interest (Peak Coordinates and Spatial Maps)

Table S1. Peak Coordinates of Components of Interest

Selected Components as Regions of Interest	X	Y	Z
Subcortical network (SC)			
Caudate (1)	6.5	10.5	5.5
Subthalamus/hypothalamus (2)	-2.5	-13.5	-1.5
Putamen (3)	-26.5	1.5	-0.5
Caudate (4)	21.5	10.5	-3.5
Thalamus (5)	-12.5	-18.5	11.5
Auditory network (AUD)			
Superior temporal gyrus ([STG], 6)	62.5	-22.5	7.5
Middle temporal gyrus ([MTG], 7)	-42.5	-6.5	10.5
Sensorimotor network (SM)			
Postcentral gyrus ([PoCG], 8)	56.5	-4.5	28.5
Left postcentral gyrus ([L PoCG], 9)	-38.5	-22.5	56.5
Paracentral lobule ([ParaCL], 10)	0.5	-22.5	65.5
Right postcentral gyrus ([R PoCG], 11)	38.5	-19.5	55.5
Superior parietal lobule ([SPL], 12)	-18.5	-43.5	65.5
Paracentral lobule ([ParaCL], 13)	-18.5	-9.5	56.5
Precentral gyrus ([PreCG], 14)	-42.5	-7.5	46.5
Superior parietal lobule ([SPL], 15)	20.5	-63.5	58.5
Postcentral gyrus ([PoCG], 16)	-47.5	-27.5	43.5
Visual network (VIS)			
Calcarine gyrus ([CalcarineG], 17)	-12.5	-66.5	8.5
Middle occipital gyrus ([MOG], 18)	-23.5	-93.5	-0.5
Middle temporal gyrus ([MTG], 19)	48.5	-60.5	10.5
Cuneus (20)	15.5	-91.5	22.5
Right middle occipital gyrus ([R MOG], 21)	38.5	-73.5	6.5
Fusiform gyrus (22)	29.5	-42.5	-12.5
Inferior occipital gyrus ([IOG], 23)	-36.5	-76.5	-4.5
Lingual gyrus ([LingualG], 24)	-8.5	-81.5	-4.5
Middle temporal gyrus ([MTG], 25)	-44.5	-57.5	-7.5
Cognitive-control network (CC)			
Inferior parietal lobule ([IPL], 26)	45.5	-61.5	43.5
Insula (27)	-30.5	22.5	-3.5
Superior medial frontal gyrus ([SMFG], 28)	-0.5	50.5	29.5
Inferior frontal gyrus ([IFG], 29)	-48.5	34.5	-0.5
Right inferior frontal gyrus ([R IFG], 30)	53.5	22.5	13.5
Middle frontal gyrus ([MiFG], 31)	-41.5	19.5	26.5
Inferior parietal lobule ([IPL], 32)	-53.5	-49.5	43.5
Right inferior parietal lobue ([R IPL], 33)	44.5	-34.5	46.5
Supplementary motor area ([SMA], 34)	-6.5	13.5	64.5
Superior frontal gyrus ([SFG], 35)	-24.5	26.5	49.5
Middle frontal gyrus ([MiFG], 36)	30.5	41.5	28.5
Hippocampus ([HiPP], 37)	23.5	-9.5	-16.5
Left inferior parietal lobule ([L IPL], 38)	-47.5	5.5	22.5
Middle cingulate cortex ([MCC], 39)	-15.5	20.5	37.5
Inferior frontal gyrus ([IFG], 40)	39.5	44.5	-0.5
Middle frontal gyrus ([MiFG], 41)	-26.5	47.5	5.5
Hippocampus ([HiPP], 42)	-24.5	-36.5	1.5
Default-mode network (DM)			
Precuneus (43)	-8.5	-66.5	35.5
Precuneus (44)	-12.5	-54.5	14.5
Anterior cingulate cortex ([ACC], 45)	-2.5	35.5	2.5
Posterior cingulate cortex ([PCC], 46)	-5.5	-28.5	26.5
Anterior cingulate cortex ([ACC], 47)	-9.5	46.5	-10.5
Precuneus (48)	-0.5	-48.5	49.5
Posterior cingulate cortex ([PCC], 49)	-2.5	54.5	31.5
Cerebellar network (CB)			
Cerebellum ([CB], 50)	-30.5	-54.5	-42.5
Cerebellum ([CB], 51)	-32.5	-79.5	-37.5
Cerebellum ([CB], 52)	20.5	-48.5	-40.5
Cerebellum ([CB], 53)	30.5	-63.5	-40.5

Table 2. Adapted from Du et al., 2020 with the breakdown of coordinates, and 53 NeuroMark ICA brain regions used for the spatially constrained ICA analysis.

Statistical Analysis

Following the analysis, loading parameter values for healthy controls, patients, and controls – patient differences were tested to identify strong/weak patterns of connectivity in the SPECT data. Group differences were calculated by performing two-sample t-tests on each of the respective 53 control/patient pairs. In addition, pairwise correlations between the loading parameters for the SPECT components were analyzed for within and between group differences.

Finally, regression models were calculated to examine relationships between clinical variables and FNC values for patients. For the regression model of interest, demographic variables such as age and sex coupled with hallucination related questions (e.g. Item 98: Hearing voices or sounds that are not real, Item 99: Experiencing Disjointed Thoughts or Speech) were examined specifically using the Amen General Symptom Checklist (GSC; https://ancronmedical.com/wp-content/uploads/2015/04/Amen-Adult-General-Symptom-Checklist.pdf), and correlated against average loading parameter values for patients. Regression models were calculated for examining these relationships between demographic and clinical variables regressed against the loading parameter matrices.

All tests were also corrected for multiple comparisons using the false discovery rate (FDR) approach[51], and t-test significant results were displayed in

connectograms to visualize the NeuroMark ICs for all 53 ICs pairings that demonstrated group differences. Analysis was performed using Matlab as well as R Studio with the base package of R ('Pile of Leaves'), version 4.4.2 (2024-10-31)[68]. ChatGPT 4-o (version 4.5) was utilized to clean, create, and streamline Matlab code [67].

A main regression model was run to understand relationships between the demographic variables and clinical items correlated with the loading parameters. Model 1 had age, sex, the clinical variables measured from items 98 and 99 regressed against the loading parameters. Sex was coded as a categorical variable, with 1 = male, 2 = female.

Model 1:

$$\text{Loading Parameters} = ß_0 + ß_1(\text{Age}) + ß_2(\text{Sex}) + ß_3(\text{Item 98}) + ß_4(\text{Item 99}) + \text{Error}$$

Additional confirmatory GLMs were run with age, sex, item 98, item 99, site, and medication status of patients on antipsychotics vs. patients not on antipsychotics. Because of the small number of patients at certain sites and the fact that controls were scanned at only one site, we were unable to control for site and medication in the full analysis, however we performed targeted analysis to evaluate the impact of site and medication. For medication, given several patients were on multiple

antipsychotic and non-antipsychotic medications, a subsample of 23 patients with no antipsychotic medication history were matched with 23 that were on antipsychotic medication. For site, we tested for site differences between sites 2 and 4, the only sites with more than 20 subjects.

Results

Part 1: Resting State SPECT Analyses

Loading Parameter Expression

We first evaluated at group differences in loading parameter expression between the 53 NeuroMark ICs. Loading parameter expression denoted how strongly an IC was expressed in each of the 53 components, with lower loading parameter values indicating less expression, and high loading parameter values indicating more expression. After FDR correction, 15 components (HC > SZ) survived with domains from every network represented. Results from the group t-test comparing healthy controls > patients using mean loading parameter values revealed connectivity in the frontal and medial temporal regions (HC > SZ). No SZ > HC differences survived FDR correction. To visually represent the FDR corrected group differences, a spatial map demonstrating the 15 loading parameters for HC > SZ was displayed below (Fig 1a) and as a bar plot demonstrating the distribution of the loading parameter values across group differences (Fig 1b). Overall loading parameter values showed intersubject functional covariance primarily in the frontal

and medial regions of the brain. For clarity, the term functional covariance will be used thoroughout to describe areas of perfusion.

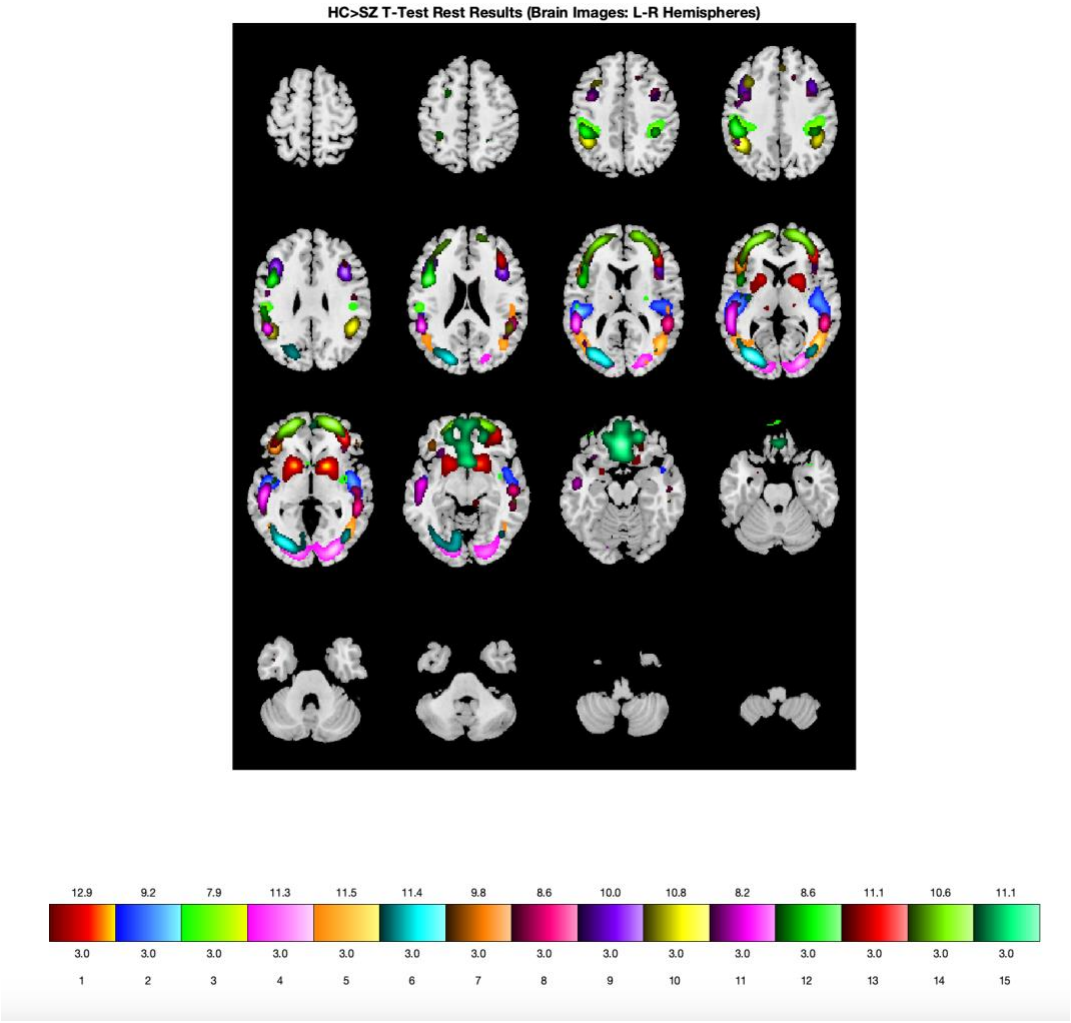

Fig 1a. A spatial map (anterior to posterior view with left and right hemispheres of the brain depicted, respectively) of corrected results (*q< 0.05)* with 15 loading parameter components showing components for healthy controls > patients, with increased loading parameter functional covariance in the frontal and medial regions of the brain.

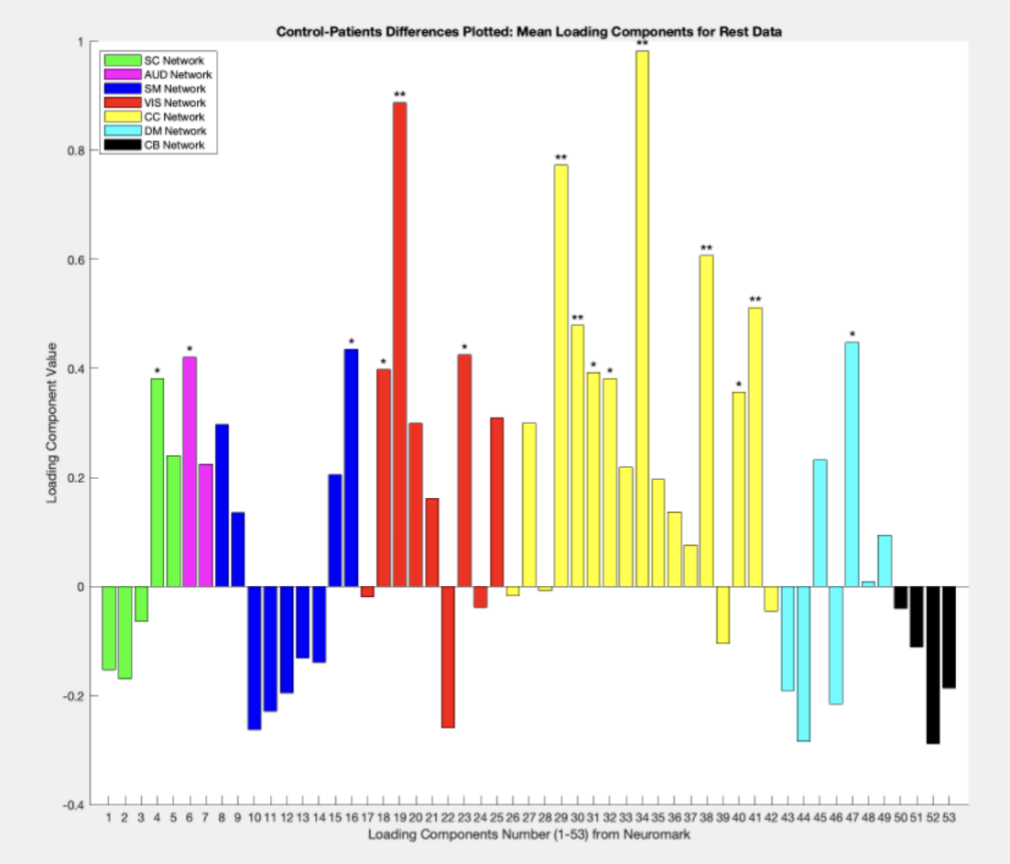

Fig 1b. A bar plot showing group differences with the corrected results (*q< 0.05)* with 15 loading parameter components showing components for healthy controls > patients . Increased loading parameter functional covariance was noted primarily in the frontal and medial regions of the brain.

FNC Results

After analyzing IC differences between groups, the next goal was to analyze interactions among networks, denoted as functional network covariation (FNC), and computed as the cross-correlation among component loading parameters. We looked

at group differences between controls vs. patients and patients vs. controls. The 7 ICNs mentioned above were investigated for broad network covariation patterns having first identified IC differences between groups in the earlier results. Weak covariation was indicated by the lighter blue colors, and strong covariation between ICNs was indicated by the orange/red colors.

Regarding broad FNC patterns (see Figs 2a and 2b), we noted that for patients (Fig 2a), higher correlations were noted for CC-DM, VIS-CB, and SM-CC networks. Weak covariation was noted for CC-CB, DM- CB, VIS-CC networks. Strong connectivity in controls (Fig 2b) was noted between the VIS-CB, VIS-DM, SM-CC, and CC-DM regions. Finally, for healthy controls-patient differences, FNC was weaker between the CC-CB, SM-CB, and SM-VIS domains (Fig 3a-3b). Regions that survived FDR correction showed weaker covariation between CC-VS, DM-CC, and DM-SM areas, and stronger covariation between the DM-SM, CC-AUD, and DM-SC areas.

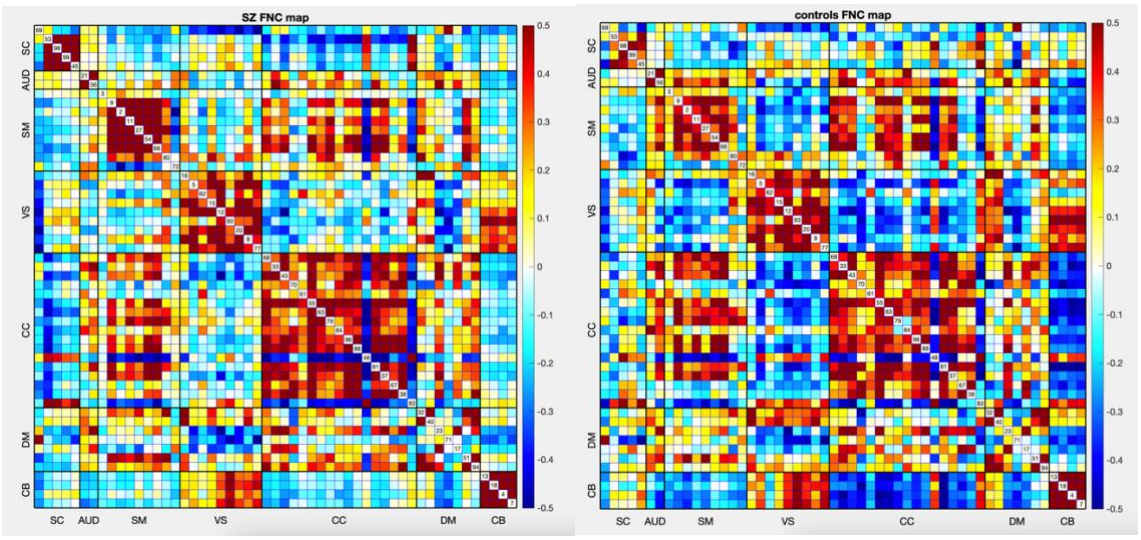

Figure 2a-2b. FNC maps of schizophrenia patients (*left*) and controls (*right*) with the NeuroMark components correlated against each other. Patient FNC maps showed strong covariation for CC-DM, VIS-CB, and SM-CC networks, and weak covariation for CC-CB, DM-CB, and VIS-CC networks. Conversely, controls showed strong connectivity between visual and CC, DM, and CB areas, but weaker connectivity in CC-CB areas.

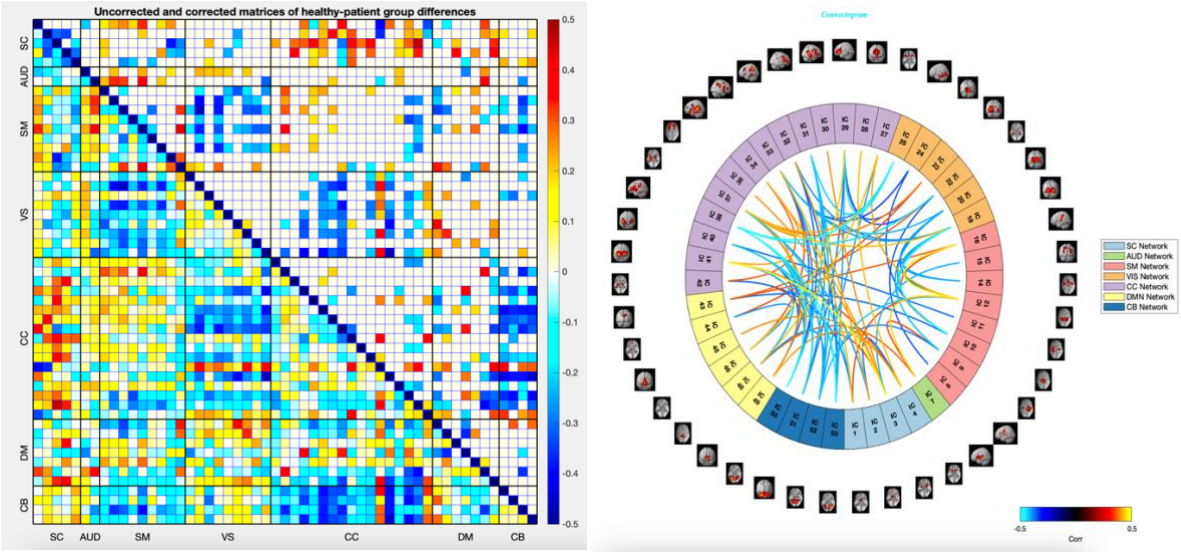

Figure 3a-3b. NeuroMark FNC map of healthy controls-patient differences (3a; left) with unthresholded (lower part of the FNC triangle) and FDR corrected results (upper part of the FNC triangle) showed stronger covariation with CC-SC, CC-AUD, and DM-AUD networks. Figure 3b (right) shows a corrected connectogram replotting the results from Figure 3a, but here allow us to see graphically which ICs are connected as well as the node strengths.

Clinical Regression Results

After identifying relevant components, relationships between loading parameters and clinical variables were examined. To do this, regressions of clinical and demographic variables against the loading parameters for patients were run. We first tested for collinearity between several clinical variables including GSC total scores (i.e. sum across all symptom severity scores in the GSC checklist), and other clinical variables related to positive and negative schizophrenia symptoms. GSC variables did not demonstrate high correlations with each other, with correlations less than 0.33.

A multiple regression was run to examine the relationship between loading parameters and clinical/demographic variables including age, sex, and hallucination symptoms (measured by Items 98 and 99 of the Amen General Symptom checklist). Overall, results (Table 3) correlating clinical symptoms to loading parameters showed relevant components (i.e. Components 27 and 28; CC Network) were strongly related to hearing voices, as well as disjointed thoughts. The other components, marginally significant at FDR corrected $q<0.1$, showed a relationship between the AUD, SM, CC, and DM networks and hallucination symptoms. Regarding the analyses run to also check for medication and site effects, there were no significant effects of either site or medication, suggesting these aspects are not of major relevance to the results.

Component	Brain Region	Q values (* q < 0.1)
GSC 98 Results		
7	Medial temporal lobe | AUD Network	0.0868
14	Precentral gyrus | SM Network	0.0865
27	Insula | CC Network	0.0100*
28	Superior medial frontal network | CC Network	0.0182*
45	Anterior cingulate cortex | DM Network	0.0647
49	Posterior cingulate cortex | DM Network	0.0957
GSC 99 Results		
3	Putamen | SC Network	0.0925
14	Precentral gyrus | SM Network	0.0980

Table 3. GSC98 and GSC99 FDR corrected $q < 0.1$ results; overall results demonstrate significance in Components 27 and 28, which are related to the CC network when correlated with hallucination symptoms. Other components, while marginally significant, demonstrate the concert of networks involved that relate to hallucination symptoms, including the CC, DM, SC, and AUD networks.

Part 2: Task Based Analyses

Loading Parameter Results

In addition to the resting state SPECT data, we compared task-based results with the CPT and the loading parameters, as well as FNC comparisons between healthy controls and patients. Bar plots were calculated to compare mean loading parameter values for healthy controls, patients, and the healthy-patient differences, with the FDR corrected results displayed. The same 15 loading parameter components for resting state were significant for the task based results. Furthermore, patients who did the CPT task showed more negative loading parameter values (i.e. reduced expression) across ICNs compared to healthy controls, who had positive loading parameter values across ICNs (i.e. increased expression; Figure 4). A spatial

map displaying the relevant components (Figures 5) with group differences are shown below.

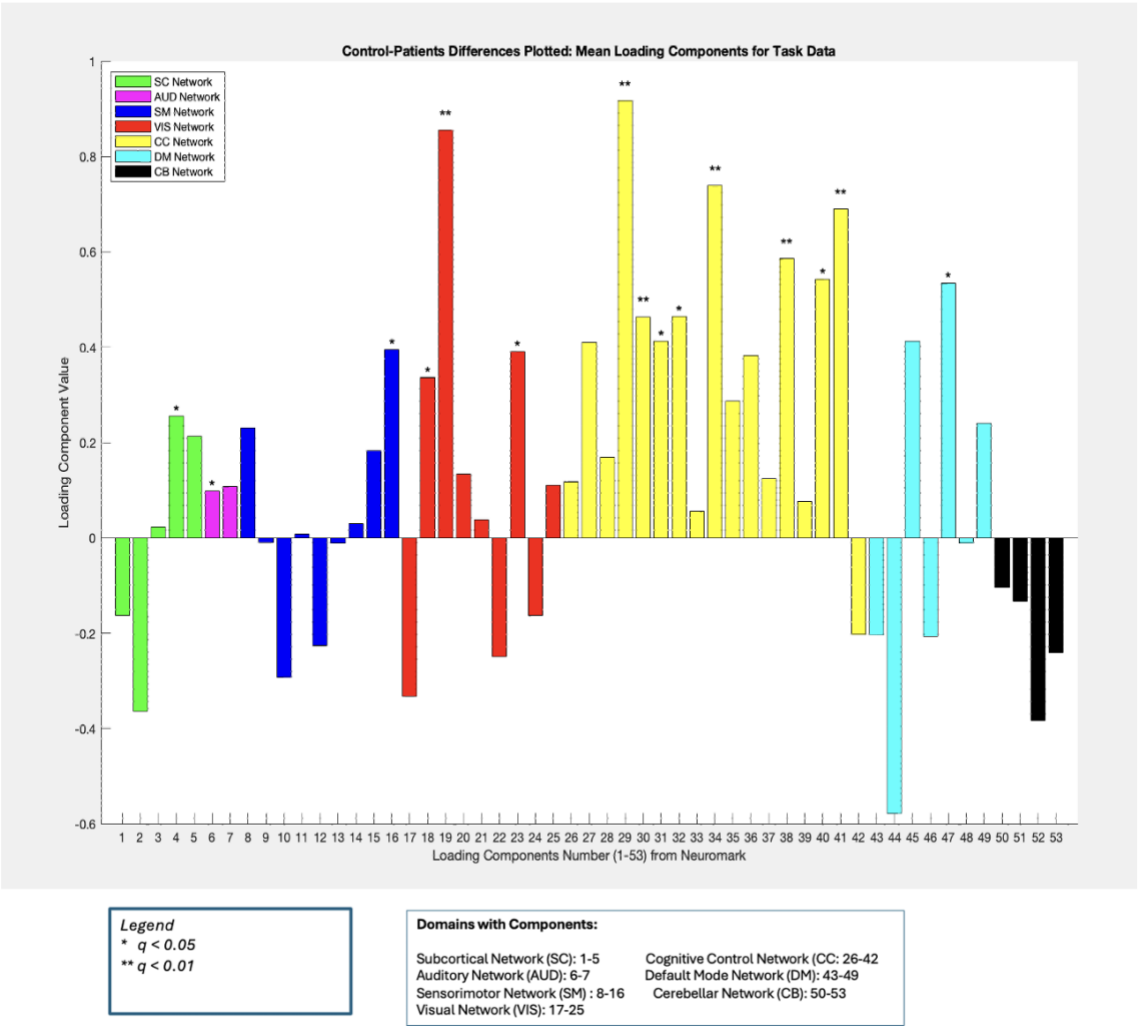

Figure 4 shows the control-patients differences in mean loading parameters for task data. Overall, patients showed reduced expression across all ICNs compared to healthy controls, which mirrored similar patterns to the resting state SPECT data.

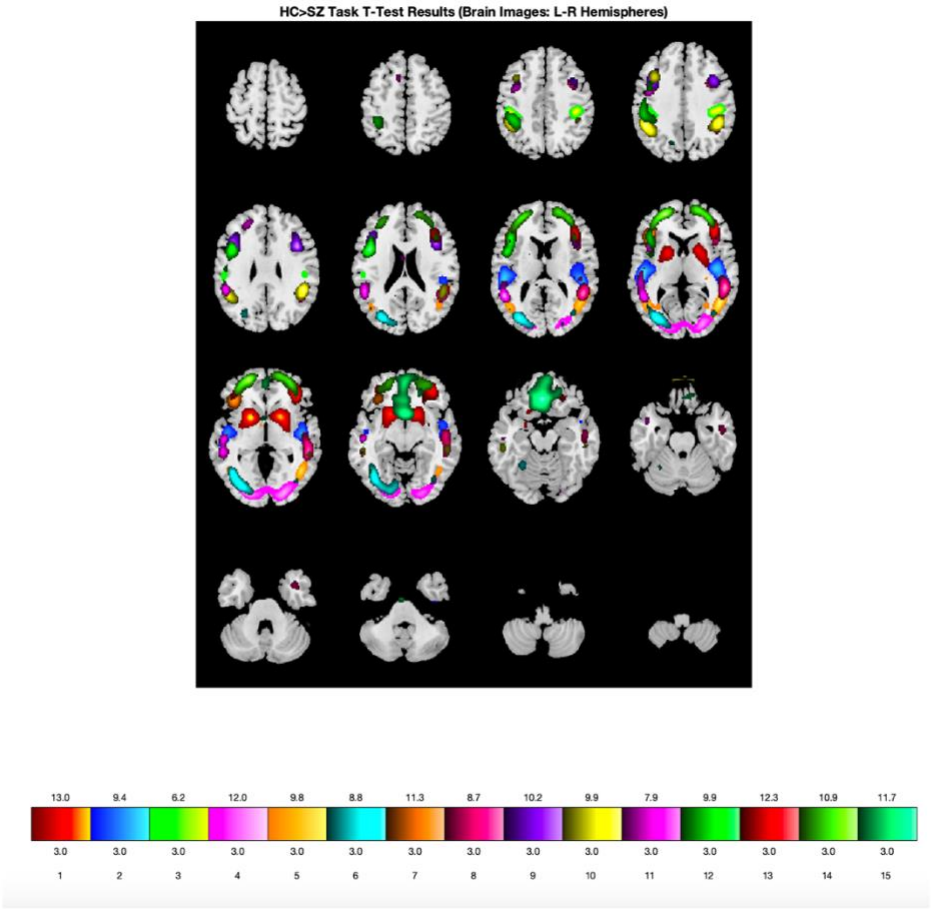

Figure 5 shows spatial maps (anterior to posterior view with left and right hemispheres of the brain depicted, respectively) of the 15 components that showed FDR corrected (*q<0.05)* significant group differences between patients and healthy controls. The results replicated across the same components identified in the resting state data. Overall, perfusion in the frontal and medial regions of the brain was present, along with broad perfusion across the 7 ICNs.

To summarize overall patterns, group differences in resting state data found 15 networks that were significant which replicated across the same components in the task data. Together, rest and task data show similar group effects with 7 common networks in the following regions: Component 4: Caudate, Component 6: Superior

Temporal Gyrus; Component 16: Postcentral Gyrus; Component 18 : Middle Occipital Gyrus, Component 19: Middle Temporal Gyrus, Component 23: Inferior Occipital Gyrus, Component 29: Inferior Frontal Gyrus, Component 30: Right Inferior Frontal Gyrus; Component 31: Middle Frontal Gyrus; Component 32: Inferior Parietal Lobule; Component 34: Supplementary Motor Area; Component 38: Left Inferior Parietal Lobule; Component 40: Inferior Frontal Gyrus; Component 41: Middle Frontal Gyrus, and Component 47: Anterior Cingulate Cortex.

FNC Task vs Rest Differences

Finally, FNC results were plotted for controls and patients to see differences between groups for rest-task FNC differences (Figures 6a-6b, 7a-7b). Patients overall showed decreased FNC as demonstrated by reduced loading parameter expression across ICNs including the CC-DM, VIS-DM, SC-CB and AUD-CB for example. By contrast, controls showed increased FNC across the 7 ICNs, namely in the VS-CB, DM-CB, and VS-CC regions. Overall, resting state data and task data compliment each other and confirm perfusion activity broadly across the 7 ICNs in the NeuroMark networks, and demonstrate differences in ICN loading parameter expression between patients and controls. When comparing rest-task data, one association survived FDR correction, namely the CC-DM association. This suggests

that despite performing an attention based task, the CC and DM areas continue to be active and engaged in both patients and healthy controls. Task based data additionally show that patients had generally reduced perfusion covariation across networks compared to healthy controls. More importantly, patients showed reduced covariation in AUD-DM, AUD-CC, VS-DM, and SC-CC networks. This suggests that as patients completed the CPT, engagement of the auditory, attention, visual, and cognitive control networks was quite reduced compared to healthy controls.

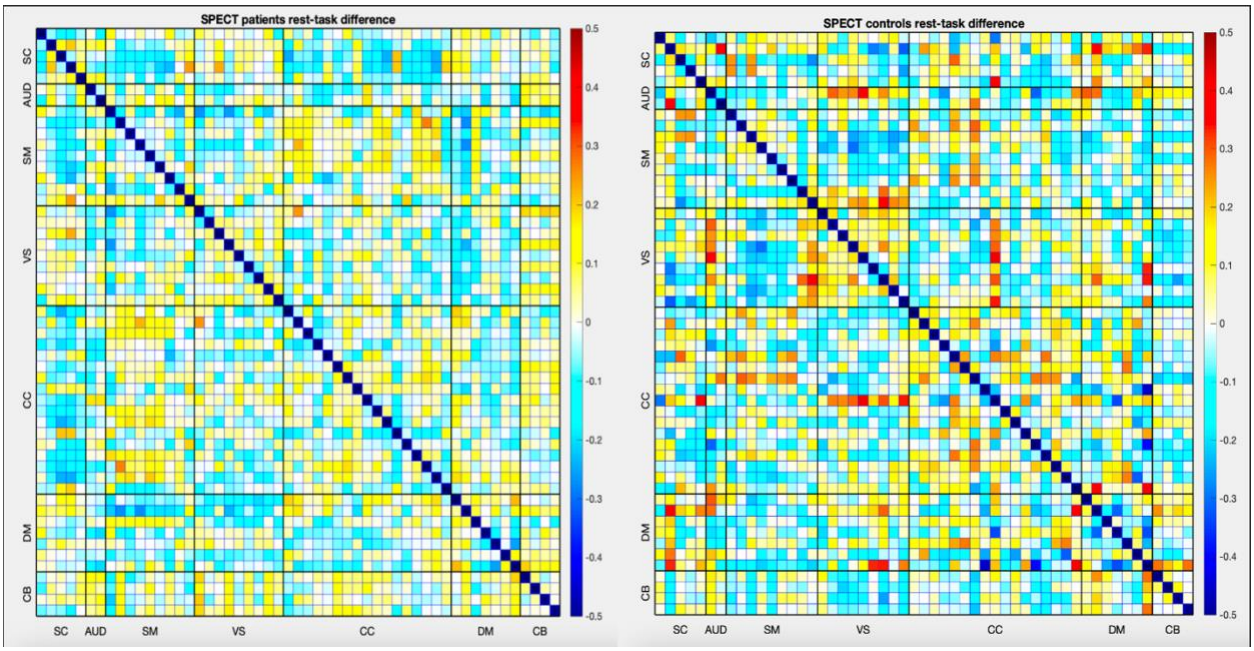

Figures 6a-6b showing FNC between SPECT patients (*left*) and healthy controls (*right*), specifically showing the resting state – task data differences. Patients showed decreased FNC compared to controls in certain networks (shown in blue hues), where controls showed increased FNC in other networks (shown in red hues).

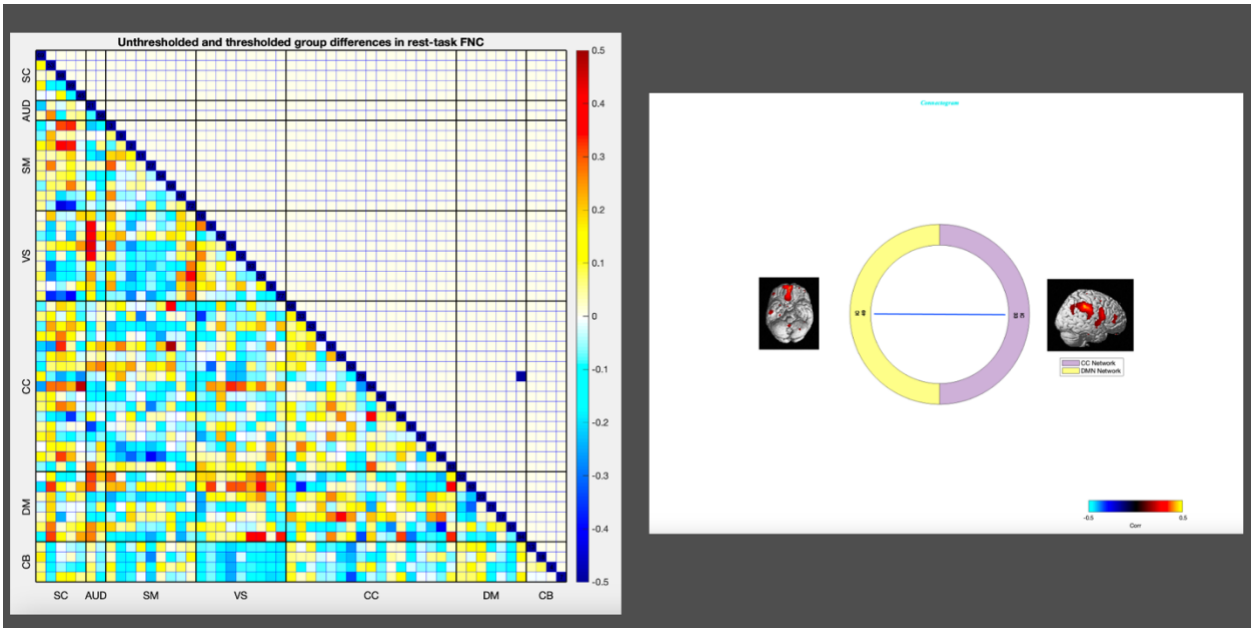

Figure 7a above shows control-patient differences with rest-task FNC matrices subtracted from eachother. Overall, increased FNC was found in networks such as the AUD-DM, VS-DM, and CC-DM areas; weaker FNC was found in regions such as the CC-CB, SM-CB, and SM-CC areas. Figure 7b highlights the corrected FDR results of the control-patient differences in rest-task data. Only one ICN association survived FDR correction, namely between the CC-DM.

Discussion and Conclusions

Here, we present the first study to utilize a NeuroMark sc-ICA approach to perform an fMRI guided analysis of SPECT data. These results show the benefits of using a fully-automated, yet flexible approach to estimate brain networks and their covariation. The significant group differences in loading parameters between healthy controls and patients are consistent with and extend prior reports [20, 53, 54,36] which indicate that variability in loading parameters is possibly linked to alterations in functional connectivity and structural disruptions. Indeed, our study noted FNC alterations across a variety of networks, including all seven of the NeuroMark

domains, but particularly in the AUD, SM, and CC domains related to clinical variables measuring age, sex, and hallucination symptoms (e.g. hearing voices). Phenomena, such as "disrupted cross talk" in patients with auditory hallucinations have been well documented [37] as disruptions in connectivity pertaining to hippocampal and auditory regions. These miscommunications stemming from disrupted connectivity could also be due to chemical imbalances, namely glutamate and GABA connectivity gone awry [35]. Interhemispheric miscommunication has been a theory in schizophrenia, and another possibility for the onset of auditory verbal hallucinations in patients. Indeed, interhemispheric miscommunication has been attributed to several causes, including possibilities of increased levels of glutamate in prefrontal and auditory regions, as well as N-methyl-D-aspartate (NMDAR) receptor dysfunctions [55].

Studies have also shown evidence of disrupted interhemispheric connectivity particularly in auditory and memory related networks, specifically decreased interhemispheric connectivity measured through voxel-mirrored homotopic connectivity (VMHC) in the STG, insula, Rolandic operculum, fusiform gyrus, and parahippocampus [38]. Taken together, these neurotransmitter dysfunctions coupled with widespread disrupted connectivity across several brain regions may explain our findings related to disrupted network connectivity across several large scale networks. Disruptions in large scale functional networks have been widely observed

with DM hypoconnectivity and relationships with DM functional connectivity and clinical symptoms a common feature [56] . We noted disruptions specifically in areas such as the parietal lobule, hippocampus, and frontal gyri which tie well with previous studies noting similar abnormalities in patients, and linking disruptions in the sensorimotor and auditory cortices [57,58,59,60] .

Other things to consider include the limitations of using HMPAO SPECT in general. It is well known that SPECT imaging has poor spatial resolution comparative to other techniques, along with costly/inefficient approvals and prior authorizations to use SPECT in medical imaging [61]. Due to poor spatial resolution of SPECT imaging, other methods such as fMRI and PET are preferred in translational clinical work[62,63], and provide much higher spatial and temporal resolution. However, it can be argued that SPECT imaging boasts high clinical accuracy[14,63,64] with techniques such as machine learning assisting with improvements in accuracy [65]. Thus, the use of SPECT in clinical settings shouldn't be completely eliminated; rather, it could be used as a complimentary tool to fMRI, PET or other measures used in neuroimaging studies.

We also noted some similarities of our results to prior fMRI work. Previous fMRI studies have found increased functional covariance in regions such as the anterior cingulate cortex and left inferior parietal lobe in PET studies [66]. Previous studies have also noted differences in connectivity between affective vs. non-

affective early phase psychosis using the NeuroMark template [41], with another PET study utilizing the NeuroMark template to provide fMRI-guided analysis of Pittsburgh Compound-B (PiB) PET data, revealing distinct patterns of covariation in mild cognitive impairment versus control subjects [66]. In studies looking at patients with FEP and early psychosis using NeuroMark, differences in FNC were found in several regions including the inferior frontal gyrus, and superior medial frontal gyrus, indicating disruptions in the cortical-subcortical-cerebellar circuits [40]. Previous ICA studies investigating disruptions in the DM, specifically abnormal dynamic functional connectivity in the precuneus and posterior cingulate cortex seem to suggest possible similarities between SPECT and fMRI methods capturing similar disruptions in connectivity [42]. Together, these results support multiple networks of dysconnectivity particularly in the cortical, cerebellar, and default mode network regions that require further exploration.

Finally, we note relationships between the CC-DM pair remain significant in a sustained attention task for healthy-patients, as well as reduced FNC patterns across the AUD, CC, DM networks in patients compared to healthy controls. This is suggestive of patients experiencing challenges with attention and focus due to the possible presence of auditory hallucinations interfering with sustained attention efforts. Previous fMRI studies using ICA have also noted relationships between hallucination symptoms and networks such as the fronto-temporal-parietal regions

[36] which broadly point to widespread disruptions of functional networks. Studies also discussed regions such as the insula, ventral striatum, hippocampus, and superior/middle temporal gyri being implicated in processes related to source monitoring and aberrant salience in schizophrenia [57]. These processes are related to aberrant cognitive perceptions that patients have about themselves and the world. The findings from our study related to decreased FNC in many of these related regions suggest that patients experience challenges with attention and general cognitive processing that need to be further explored. Given that controls had stronger FNC with the same networks, it could be that they were able to focus more extensively on the task without the interference of hallucinations affecting these cognitive states. However, given that it is not clear how frequent and if hallucinations were present in patients at the time of the attention task – more research in this domain is needed to fully understand these patterns.

Some of the limitations of this study included not having other SPECT covariation studies in schizophrenia to which to compare results. While a novel study such as this one is promising, more translational and clinical research in schizophrenia using SPECT imaging is needed to extend these findings to other datasets or populations, including, but not limited to comorbid populations. Future directions should utilize large scale datasets and also do comparative ICA processes similar to this study to see if results replicate.

Another limitation was controlling across the different sites and scanner type given participants were scanned with both scanners across sites, accounting for variable subject totals across site, and finally accounting for subjects on antipsychotics across site. Table 1a clearly shows the breakdown of subjects across site, particularly the limited samples across some sites. Because controls were all collected at one site, and small numbers of patients were collected at the other clinic sites, we observed that it was a challenge to control for site as a covariate. However, we tested for group differences between patients collected at the two largest sites and found no differences, which suggests that site is not a major factor in driving the results. The other challenge was controlling for medication status. Some patients had multiple medication statuses (e.g. being on antipsychotics and non-antipsychotics) which left a small sample size to further analyze this covariate. To account for this, we compared patients on multiple medications versus those that were not on any medications. Despite adjusting for this, no results survived. Therefore, a larger sample size of medicated patients solely on antipsychotics is needed to further analyze the effects of antipsychotics on perfusion data.

In conclusion, analyzing SPECT data using ICA revealed multiple significant group differences in HC vs SZ. This poses interesting clinical questions related to possible disruptions in schizophrenia, particularly in the superior temporal gyrus, default mode network, and subcortical networks. Given that this is the first fMRI

guided network-based analysis of SPECT data, these results shed further light on patterns of functional dysconnectivity identified in various studies relating disruption in these networks correlated with positive and negative symptoms in schizophrenia. Thus, findings from this study can be taken as a first step to conduct future SPECT and other modality related studies to compare FNC in schizophrenia. Taken together with clinical data, we hope to further analyze the SPECT data to see how group differences emerge across a variety of neuropsychiatric disorders. In conclusion, utilizing SPECT imaging could be a useful complement to existing fMRI research in finding novel biomarkers of schizophrenia.

Disclosure | Conflict of Interest Statements

The imaging data was collected by the Amen Clinics as part of their routine patient intake for clinical treatment. Upon consent (Integ Review Board (004-Amen Clinics Inc.)), patients provide their de-identified data for research use, made available by the non-profit Change Your Brain Foundation to academic and research institutions.

TReNDS used the retrospective imaging data from Change Your Brain Foundation to study functional connectivity in schizophrenia across imaging modalities.

Dr. Keator is currently a research scientist at the Amen Clinic, and receives a salary from the clinic to perform neuroimaging research. Dr. Amen is the founder and CEO of Amen Clinics, receives salary, and owns private stock of the company.

Data/Code Availability Statement

Due to the sensitive nature of this clinical data, the SPECT data has not been posted publicly but the anonymized demographic and other clinical data used in this study is freely available for research by request to Dr. Keator. The code in MATLAB and R, and other associated files are available on Github: (https://github.com/trendscenter/gift-bids/tree/main/misc/spect/proj/march2024).

References

1. Bondi E, Maggioni E, Brambilla P, Delvecchio G. A systematic review on the potential use of machine learning to classify major depressive disorder from healthy controls using resting state fMRI measures. *Neurosci Biobehav Rev*. 2023;144:104972. doi:10.1016/j.neubiorev.2022.104972

2. Lee MH, Smyser CD, Shimony JS. Resting state fMRI: A review of methods and clinical applications. *AJNR Am J Neuroradiol*. 2014;34(10):1866-1872. doi:10.3174/ajnr.A3263.Resting

3. Biswal B, Yetkin FZ, Haughton VM, Hyde JS. Functional connectivity in the motor cortex of resting human brain using echo-planar MRI. *Magn Reson Med Off J Soc Magn Reson Med Soc Magn Reson Med*. 1995;34(4):537-541. doi:10.1002/mrm.1910340409

4. van den Heuvel MP, Hulshoff Pol HE. Exploring the brain network: A review on resting-state fMRI functional connectivity. *Eur Neuropsychopharmacol*. 2010;20(8):519-534. doi:10.1016/j.euroneuro.2010.03.008

5. Dennis EL, Thompson PM. Mapping connectivity in the developing brain. *Int J Dev Neurosci*. 2013;31(7):525-542. doi:10.1016/j.ijdevneu.2013.05.007

6. Fox MD, Greicius M. Clinical applications of resting state functional connectivity. *Front Syst Neurosci*. 2010;4(June):19. doi:10.3389/fnsys.2010.00019

7. Koyama M, Kawashima R, Ito H, et al. SPECT Imaging of Normal Subjects with Technetium-99m-HMPAO and Technetium-99m-ECD.

8. Galiana Á, Paredes I, Ruiz S, et al. *Effects of Cranioplasty in Cerebral Blood Perfusion Using Quantification with 99mTc-HMPAO SPECT-CT*. In Review; 2021. doi:10.21203/rs.3.rs-539070/v1

9. Sabouri M, Hajianfar G, Hosseini Z, et al. Myocardial Perfusion SPECT Imaging Radiomic Features and Machine Learning Algorithms for Cardiac Contractile Pattern Recognition. *J Digit Imaging*. 2022;36(2):497-509. doi:10.1007/s10278-022-00705-9

10. Percie Du Sert O, Unrau J, Gauthier CJ, et al. Cerebral blood flow in schizophrenia: A systematic review and meta-analysis of MRI-based studies. *Prog Neuropsychopharmacol Biol Psychiatry*. 2023;121:110669. doi:10.1016/j.pnpbp.2022.110669

11. Zhu J, Zhuo C, Qin W, et al. Altered resting-state cerebral blood flow and its connectivity in schizophrenia. *J Psychiatr Res*. 2015;63:28-35. doi:10.1016/j.jpsychires.2015.03.002

12. Selvaggi P, Jauhar S, Kotoula V, et al. Reduced cortical cerebral blood flow in antipsychotic-free first-episode psychosis and relationship to treatment response. *Psychol Med*. 2023;53(11):5235-5245. doi:10.1017/S0033291722002288

13. Boisvert M, Lungu O, Pilon F, Dumais A, Potvin S. Regional cerebral blood flow at rest in schizophrenia and major depressive disorder: A functional neuroimaging meta-analysis. *Psychiatry Res Neuroimaging*. 2023;335:111720. doi:10.1016/j.pscychresns.2023.111720

14. Amen DG, Trujillo M, Newberg A, et al. Brain SPECT Imaging in Complex Psychiatric Cases: An Evidence-Based, Underutilized Tool. *Open Neuroimaging J*. 2011;5:40-48. doi:10.2174/1874440001105010040

15. Premi E, Calhoun VD, Garibotto V, et al. Source-Based Morphometry Multivariate Approach to Analyze [123I]FP-CIT SPECT Imaging. *Mol Imaging Biol*. 2017;19(5):772-778. doi:10.1007/s11307-017-1052-3

16. Xiongchao Chen, Bo Zhou, Huidong Xie, et al. Deep Learning-Based Attenuation Map Generation for Low-Dose and Few-Angle Dedicated Cardiac SPECT. *J Nucl Med*. 2023;64(supplement 1):P802.

17. Khachnaoui H, Mabrouk R, Khlifa N. Machine learning and deep learning for clinical data and PET/SPECT imaging in Parkinson's disease: a review. *IET Image Process*. 2020;14(16):4013-4026. doi:10.1049/iet-ipr.2020.1048

18. Scherfler C, Seppi K, Donnemiller E, et al. Voxel-wise analysis of [123I]β-CIT SPECT differentiates the Parkinson variant of multiple system atrophy from idiopathic Parkinson's disease. *Brain*. 2005;128(7):1605-1612. doi:10.1093/brain/awh485

19. Du Y, Pearlson GD, Liu J, et al. A group ICA based framework for evaluating resting fMRI markers when disease categories are unclear: application to schizophrenia, bipolar, and schizoaffective disorders. *NeuroImage*. 2015;122:272-280. doi:10.1016/j.neuroimage.2015.07.054

20. Calhoun VD. Functional brain networks in schizophrenia: a review. *Front Hum Neurosci*. 2009;3. doi:10.3389/neuro.09.017.2009

21. Harikumar A, Solovyeva KP, Misiura M, et al. Revisiting Functional Dysconnectivity: a Review of Three Model Frameworks in Schizophrenia. *Curr Neurol Neurosci Rep*. 2023;23(12):937-946. doi:10.1007/s11910-023-01325-8

22. Calhoun VD, Allen E. Extracting Intrinsic Functional Networks with Feature-Based Group Independent Component Analysis. *Psychometrika*. 2013;78(2):243-259. doi:10.1007/s11336-012-9291-3

23. Bell AJ, Sejnowski TJ. An information-maximisation approach to blind separation and blind deconvolution.

24. Mckeown MJ, Makeig S, Brown GG, et al. Analysis of fMRI data by blind separation into independent spatial components. *Hum Brain Mapp*. 1998;6(3):160-188. doi:10.1002/(SICI)1097-0193(1998)6:3<160::AID-HBM5>3.0.CO;2-1

25. Calhoun VD, Adali T, Pearlson GD, Pekar JJ. A method for making group inferences from functional MRI data using independent component analysis. *Hum Brain Mapp*. 2001;14(3):140-151. doi:10.1002/hbm.1048

26. Calhoun VD. Functional brain networks in schizophrenia: a review. *Front Hum Neurosci*. 2009;3. doi:10.3389/neuro.09.017.2009

27. for the Alzheimer's Disease Neuroimaging Initiative (ADNI), Luo X, Jiaerken Y, et al. Affect of APOE on information processing speed in non-demented elderly population: a preliminary structural MRI study. *Brain Imaging Behav*. 2017;11(4):977-985. doi:10.1007/s11682-016-9571-0

28. Maddahi J, Agostini D, Bateman TM, et al. Flurpiridaz F-18 PET Myocardial Perfusion Imaging in Patients With Suspected Coronary Artery Disease. *J Am Coll Cardiol*. 2023;82(16):1598-1610. doi:10.1016/j.jacc.2023.08.016

29. Fang XT, Toyonaga T, Hillmer AT, et al. Identifying brain networks in synaptic density PET (11C-UCB-J) with independent component analysis. *NeuroImage*. 2021;237:118167. doi:10.1016/j.neuroimage.2021.118167

30. Du Y, Fryer SL, Lin D, et al. Identifying functional network changing patterns in individuals at clinical high-risk for psychosis and patients with early illness schizophrenia: A group ICA study. *NeuroImage Clin*. 2018;17:335-346. doi:10.1016/j.nicl.2017.10.018

31. Salman MS, Du Y, Lin D, et al. Group ICA for identifying biomarkers in schizophrenia: 'Adaptive' networks via spatially constrained ICA show more sensitivity to group differences than spatio-temporal regression. *NeuroImage Clin*. 2019;22:101747. doi:10.1016/j.nicl.2019.101747

32. Duda M, Iraji A, Ford JM, et al. *Spatially Constrained ICA Enables Robust Detection of Schizophrenia from Very Short Resting-State fMRI Data*. Psychiatry and Clinical Psychology; 2022. doi:10.1101/2022.03.17.22271783

33. Du Y, Fu Z, Sui J, et al. NeuroMark: An automated and adaptive ICA based pipeline to identify reproducible fMRI markers of brain disorders. *NeuroImage Clin*. 2020;28:102375. doi:10.1016/j.nicl.2020.102375

34. Gao J, Zhang D, Wang L, et al. Altered Effective Connectivity in Schizophrenic Patients With Auditory Verbal Hallucinations: A Resting-State fMRI Study With Granger Causality Analysis. *Front Psychiatry*. 2020;11:575. doi:10.3389/fpsyt.2020.00575

35. Weber S, Hjelmervik H, Craven AR, et al. Glutamate- and GABA-Modulated Connectivity in Auditory Hallucinations—A Combined Resting State fMRI and MR Spectroscopy Study. *Front Psychiatry*. 2021;12:643564. doi:10.3389/fpsyt.2021.643564

36. Kubera KM, Rashidi M, Schmitgen MM, et al. Structure/function interrelationships in patients with schizophrenia who have persistent auditory verbal hallucinations: A multimodal MRI study using parallel ICA. *Prog Neuropsychopharmacol Biol Psychiatry*. 2019;93:114-121. doi:10.1016/j.pnpbp.2019.03.007

37. Hare SM, Law AS, Ford JM, et al. Disrupted network cross talk, hippocampal dysfunction and hallucinations in schizophrenia. *Schizophr Res*. 2018;199:226-234. doi:10.1016/j.schres.2018.03.004

38. Chen C, Huang H, Qin X, et al. Reduced inter-hemispheric auditory and memory-related network interactions in patients with schizophrenia experiencing auditory verbal hallucinations. *Front Psychiatry*. 2022;13:956895. doi:10.3389/fpsyt.2022.956895

39. Dierckx RAJO, Otte A, De Vries EFJ, Van Waarde A, Sommer IE, eds. *PET and SPECT in Psychiatry*. Springer International Publishing; 2021. doi:10.1007/978-3-030-57231-0

40. Jensen KM, Calhoun VD, Fu Z, et al. A whole-brain neuromark resting-state fMRI analysis of first-episode and early psychosis: Evidence of aberrant cortical-subcortical-cerebellar functional circuitry. *NeuroImage Clin*. 2024;41:103584. doi:10.1016/j.nicl.2024.103584

41. Fu Z, Iraji A, Sui J, Calhoun VD. Whole-brain functional network connectivity abnormalities in affective and non-affective early phase psychosis. *Front Neurosci*. 2021;15:682110.

42. Sendi MSE, Zendehrouh E, Ellis CA, et al. Aberrant Dynamic Functional Connectivity of Default Mode Network in Schizophrenia and Links to Symptom Severity. *Front Neural Circuits*. 2021;15:649417. doi:10.3389/fncir.2021.649417

43. Conners CK. *Conners' Continuous Performance Test*. Multi-health systems North Tonawanda NY; 2000.

44. Chang LT. A Method for Attenuation Correction in Radionuclide Computed Tomography. *IEEE Trans Nucl Sci*. 1978;25(1):638-643. doi:10.1109/TNS.1978.4329385

45. Chang W, Henkin RE, Buddemeyer E. The Source of Overestimation in the Quantification by SPECT of Uptakes in. *J Nucl Med*. 1984;25:788-791.

46. Avants BB, Tustison NJ, Song G, Cook PA, Klein A, Gee JC. A reproducible evaluation of ANTs similarity metric performance in brain image registration. *NeuroImage*. 2011;54(3):2033-2044. doi:10.1016/j.neuroimage.2010.09.025

47. Fonov VS, Evans AC, McKinstry RC, Almli CR, Collins DL. Unbiased nonlinear average age-appropriate brain templates from birth to adulthood. *NeuroImage*. 2009;47:S102.

48. Fonov V, Evans AC, Botteron K, et al. Unbiased average age-appropriate atlases for pediatric studies. *Neuroimage*. 2011;54(1):313-327.

49. Matlab S. Matlab. *MathWorks Natick MA*. Published online 2012.

50. Du Y, Fu Z, Sui J, et al. NeuroMark: An automated and adaptive ICA based pipeline to identify reproducible fMRI markers of brain disorders. *NeuroImage Clin*. 2020;28:102375. doi:10.1016/j.nicl.2020.102375

51. Benjamini Y, Hochberg Y. Controlling the False Discovery Rate: A Practical and Powerful Approach to Multiple Testing. *J R Stat Soc Ser B Stat Methodol*. 1995;57(1):289-300. doi:10.1111/j.2517-6161.1995.tb02031.x

52. Team RDC. R: A language and environment for statistical computing. *No Title*. Published online 2010.

53. Duda M, Faghiri A, Belger A, et al. *Alterations in Grey Matter Structure Linked to Frequency-Specific Cortico-Subcortical Connectivity in Schizophrenia via Multimodal Data Fusion*. Neuroscience; 2023. doi:10.1101/2023.07.05.547840

54. Jensen DM, Zendrehrouh E, Calhoun V, Turner JA. Cognitive Implications of Correlated Structural Network Changes in Schizophrenia. *Front Integr Neurosci*. 2022;15:755069. doi:10.3389/fnint.2021.755069

55. Steinmann S, Leicht G, Mulert C. The interhemispheric miscommunication theory of auditory verbal hallucinations in schizophrenia. *Int J Psychophysiol*. 2019;145:83-90. doi:10.1016/j.ijpsycho.2019.02.002

56. O'Neill A, Mechelli A, Bhattacharyya S. Dysconnectivity of Large-Scale Functional Networks in Early Psychosis: A Meta-analysis. *Schizophr Bull*. 2019;45(3):579-590. doi:10.1093/schbul/sby094

57. Kowalski J, Aleksandrowicz A, Dąbkowska M, Gawęda Ł. Neural Correlates of Aberrant Salience and Source Monitoring in Schizophrenia and At-Risk Mental States—A Systematic Review of fMRI Studies. *J Clin Med*. 2021;10(18):4126. doi:10.3390/jcm10184126

58. Das TK, Kumar J, Francis S, Liddle PF, Palaniyappan L. Parietal lobe and disorganisation syndrome in schizophrenia and psychotic bipolar disorder: A bimodal

connectivity study. *Psychiatry Res Neuroimaging*. 2020;303:111139. doi:10.1016/j.pscychresns.2020.111139

59. Dabiri M, Dehghani Firouzabadi F, Yang K, Barker PB, Lee RR, Yousem DM. Neuroimaging in schizophrenia: A review article. *Front Neurosci*. 2022;16:1042814. doi:10.3389/fnins.2022.1042814

60. Clark SV, Tannahill A, Calhoun VD, Bernard JA, Bustillo J, Turner JA. Weaker Cerebellocortical Connectivity Within Sensorimotor and Executive Networks in Schizophrenia Compared to Healthy Controls: Relationships with Processing Speed. *Brain Connect*. 2020;10(9):490-503. doi:10.1089/brain.2020.0792

61. Bateman TM. Advantages and disadvantages of PET and SPECT in a busy clinical practice. *J Nucl Cardiol*. 2012;19:3-11. doi:10.1007/s12350-011-9490-9

62. Ingram M, Colloby SJ, Firbank MJ, Lloyd JJ, O'Brien JT, Taylor JP. Spatial covariance analysis of FDG-PET and HMPAO-SPECT for the differential diagnosis of dementia with Lewy bodies and Alzheimer's disease. *Psychiatry Res Neuroimaging*. 2022;322:111460. doi:10.1016/j.pscychresns.2022.111460

63. Henderson TA, Cohen P, Van Lierop M, et al. A Reckoning to Keep Doing What We Are Already Doing With PET and SPECT Functional Neuroimaging. *Am J Psychiatry*. 2020;177(7):637-638. doi:10.1176/appi.ajp.2020.19080801

64. Amen DG, Easton M. A New Way Forward: How Brain SPECT Imaging Can Improve Outcomes and Transform Mental Health Care Into Brain Health Care. *Front Psychiatry*. 2021;12:715315. doi:10.3389/fpsyt.2021.715315

65. Fard AS, Reutens DC, Ramsay SC, Goodman SJ, Ghosh S, Vegh V. Image synthesis of interictal SPECT from MRI and PET using machine learning. *Front Neurol*. 2024;15:1383773. doi:10.3389/fneur.2024.1383773

66. Saha DK, Bohsali A, Saha R, Hajjar I, Calhoun VD. *Neuromark PET: A Multivariate Method for Estimating and Comparing Whole Brain Functional Networks and Connectomes from fMRI and PET Data*. Neuroscience; 2024. doi:10.1101/2024.01.10.575131

67. OpenAI. (2024). *ChatGPT (November 2024 version)* [Large language model]. OpenAI. https://chat.openai.com/

68. R Core Team. (2024). *R: A language and environment for statistical computing*. R Foundation for Statistical Computing. https://www.R-project.org/

69. Jutten, C. (1988). Independent component analysis versus PCA. *Proceeding of European Signal Processing Conferemce, 1988*.